Ⓔ

Evidence for a Twelfth Large Earthquake on the Southern Hayward Fault in the Past 1900 Years

by James J. Lienkaemper, Patrick L. Williams, and Thomas P. Guilderson

Abstract   We present age and stratigraphic evidence for an additional paleoearthquake at the Tyson Lagoon site. The acquisition of 19 additional radiocarbon dates and the inclusion of this additional event has resolved a large age discrepancy in our earlier earthquake chronology. The age of event E10 was previously poorly constrained, thus increasing the uncertainty in the mean recurrence interval (RI), a critical factor in seismic hazard evaluation. Reinspection of many trench logs revealed substantial evidence suggesting that an additional earthquake occurred between E10 and E9 within unit u45. Strata in older u45 are faulted in the main fault zone and overlain by scarp colluviums in two locations. We conclude that an additional surface-rupturing event (E9.5) occurred between E9 and E10. Since 91 A.D. (± 40 yr, 1σ), 11 paleoearthquakes preceded the M 6.8 earthquake in 1868, yielding a mean RI of 161 ± 65 yr (1σ, standard deviation of recurrence intervals). However, the standard error of the mean (SEM) is well determined at ± 10 yr. Since ~1300 A.D., the mean rate has increased slightly, but is indistinguishable from the overall rate within the uncertainties. Recurrence for the 12-event sequence seems fairly regular: the coefficient of variation is 0.40, and it yields a 30-yr earthquake probability of 29%. The apparent regularity in timing implied by this earthquake chronology lends support for the use of time-dependent renewal models rather than assuming a random process to forecast earthquakes, at least for the southern Hayward fault.

Online Material: Twelve-event Oxcal model for paleoearthquakes of the Hayward fault.

Introduction

In this third of three related reports (this paper; Lienkaemper *et al.*, 2002a [L02]; and Lienkaemper and Williams, 2007 [LW07]), we present evidence for a previously unrecognized earthquake within a millennial record of earthquakes for the southern Hayward fault (HS) at Tyson's Lagoon (Fig. 1). The brevity of the continuous historical record in the San Francisco Bay area, 230 yr at most, makes the determination of earthquake recurrence from geologic evidence of past large earthquakes especially critical to regional seismic hazard analysis (e.g., Working Group on California Earthquake Probabilities, 2003 and 2008, hereafter abbreviated as WG03 and WG08).

A thorough introduction and detailed documentation for this overall earthquake chronology has already been presented in L02 and LW07; field data are available in Lienkaemper *et al.*, 2002b, 2003, 2005. Here we present only new interpretations of evidence supporting an additional paleoearthquake (Fig. 2a,b) and its stratigraphic position (Fig. 2c), the new radiocarbon data (Table 1, Fig. 2), and the results of the revised Oxcal chronologic model (Table 2, Figs. 3–6).

Our previous paper, LW07, presented evidence for at least 11 earthquakes at Tyson's Lagoon site during the past two millennia, including the 1868 historical earthquake. Recently, we were given the opportunity to date additional radiocarbon samples (Table 1); we directed our attention to the most poorly constrained earthquake age, event E10. Because many appropriate samples were still available, this appeared to offer the best chance for improving the overall chronology.

Evidence for an Additional Paleoearthquake

The recalculation of the LW07 chronologic model using the Bayesian statistical computer program Oxcal (Bronk Ramsey, 1995, 2001, 2007), now including eight of the new samples, resulted in a well-constrained age of E10. As part of the process of obtaining additional age control for E10, we began a review of all trench logs and upon close inspection, recognized evidence suggesting the existence of an event that had previously been overlooked.
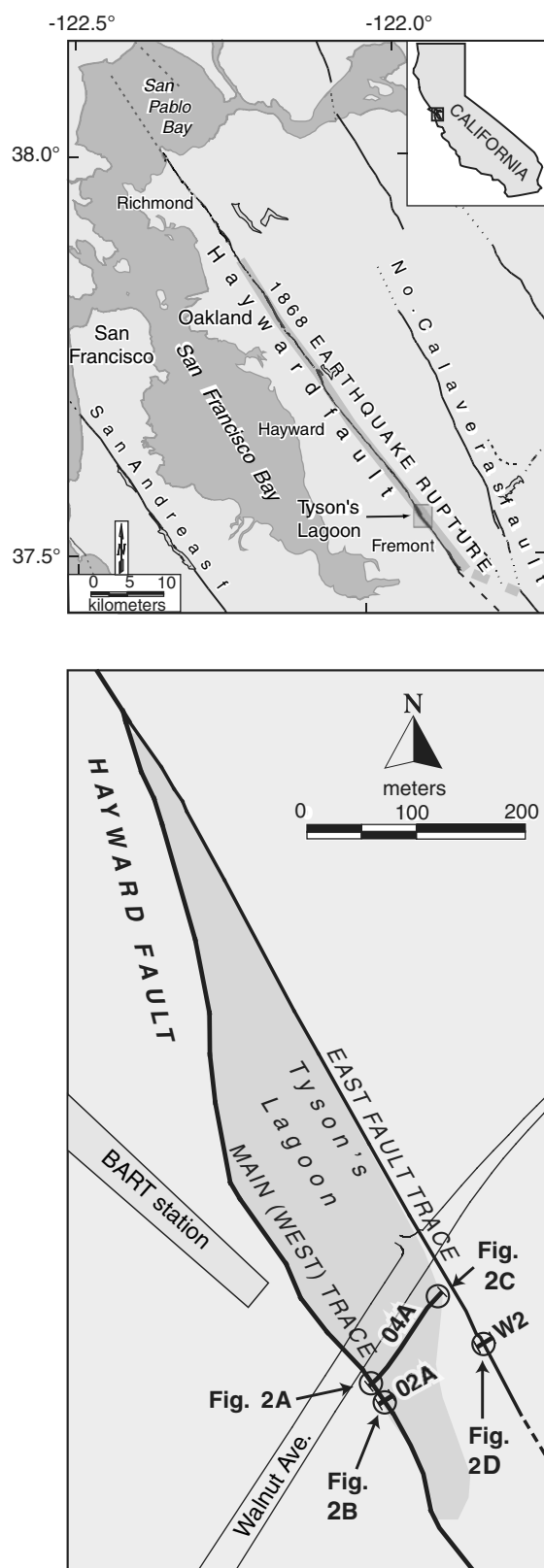
Figure 1. Site location maps. (a) The gray band along the Hayward fault from Oakland to Fremont indicates the approximate extent of the 1868 rupture (Lienkaemper and Galehouse, 1998). (b) Circles indicate the locations of the trench logs shown in Figure 2.

Figure 2a shows the strongest evidence for an intervening earthquake, E9.5, a blocky scarp colluvium (highlighted in orange) within unit u45 observed at the main fault in the south wall of trench 04A (location shown in Fig. 1). We regard blocky scarp colluvium as the most certain indication of a surface-rupturing earthquake, as distinguished from aseismic slip or creep, which also occurs on the Hayward fault at this location. Similar blocky colluvium figures prominently in event evidence for events E7, E8, E10, and E11 (LW07 Table 2). This colluvium directly overlies a 0.07 m wide shear zone, which must have moved last during the same rupture event because it does not penetrate overlying layers. Other fault traces with substantial vertical separations exist upslope, and the associated scarps probably contributed to the blocky scarp colluvium, although we recognize that these traces may have moved again in subsequent events. The small thickness of colluvium is not unusual for earthquakes at this site because the strike-slip component of slip is much larger than the local vertical component. We surmise that the colluvium formed in a zone of distributed oblique-slip shears as the sheared material cascaded downslope or was transported by later storm runoff.

Another scarp colluvium is located within unit u45 in another trench, 02A (location shown in Fig. 1, log detail in Fig. 2b). Although not identified as blocky in texture, this colluvium is thickest at and overlies one of the most active fault traces and is absent away from the scarp. This is unlike the much broader distribution of colluvium expected downslope from a creeping fault trace (L02). On both sides of the fault, the colluvium is composed of two parts: (1) a thicker lower part of clayey silt derived from underlying older u45, and (2) a thinner upper part of coarsely stratified sand and soil fragments. The slightly beveled corner of the upper block of u45 at the fault trace is consistent with the collapse of a small free face. The upper sandy colluvium presumably formed due to continuing erosion of the material at this and other traces within a broader zone of vertical deformation above (Fig. 2b). Further evidence of E9.5 is that the block of older u45 beneath the colluvium appears distinctly more tilted than overlying units, including the younger part of u45. The scarp colluvium in trench 02A has been altered by prolonged saturation, so its original texture may or may not have been blocky. However, it is distinctly thickest only in the immediate vicinity of faults with sizeable vertical separation (Fig. 2b). It is also associated with distinct tectonic tilting not in evidence in upper u45. Finally, the size and shape of this colluvium is similar to others where the blocky character could be distinguished.

Additional support for E9.5 includes upward terminating fault strands within unit u45 at four other locations. (1) In trench 02A (north wall, m8; Lienkaemper *et al.*, 2003, sheet 2), the base of u45 is equivocally offset by 0.25 m, but the top of u45 is not offset; however, the base of u41 does not corroborate this much vertical separation here. (2) In trench 01A (north wall, m8; Lienkaemper *et al.*, 2003, sheet 1), unit u41 is conspicuously offset, but the top of u45 is clearly not
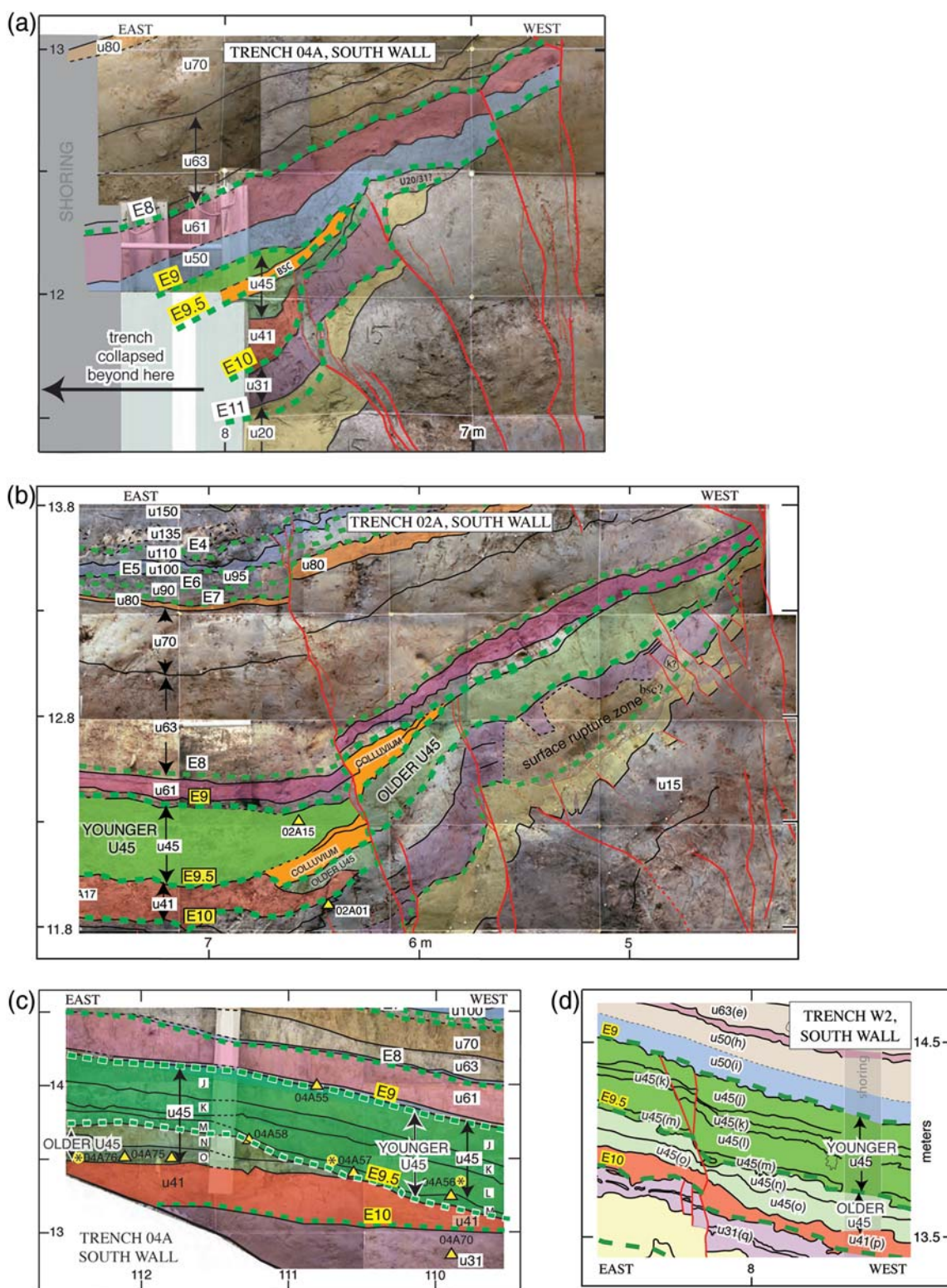
Figure 2. (a) Log of part of the south wall of trench 04A at the main fault along the western edge of Tyson's Lagoon, showing faults in red and event horizons (E8 to E11) as dashed green lines. Stratigraphic units are numbered: for example, u20, u45, etc. The orange blocky scarp colluvium (BSC) in unit u45 is interpreted to have been produced by event E9.5 and is further described in the text. (b) Log of part of the south wall of trench 02A. Colluvium within unit u45 in this exposure, although not visibly blocky, formed only on the fault scarp, so we conclude that it formed during and just after earthquake E9.5. (c) Log of part of the south wall of trench 04A about 105 m east of the main fault trace. This trench shows erosional unconformity between younger u45 (J, K, L, M) and older u45 (N, O). Yellow triangles indicate carbon samples; asterisks indicate samples dated for this study. (d) Log of part of the south wall of trench W2 (1992; Lienkaemper et al., 2003), E9 event horizon at the top of u45 (J).

Table 1
Radiocarbon Ages of Additional Charcoal Samples Dated for This Study

Sample Number*	14C Age (yr) BP, Corrected[†]	Unit Number	Wall	Location (y-Axis, m)	δ13C[‡]	Fraction Modern	D14C	Lab. Number[§]
04A-7a	1895 ± 30	41 (p)	s	31	−25.5	0.7899 ± 0.0026	−210.1	135736
04A-7a rep	1840 ± 30	41 (p)	s	31	−25.5	0.7951 ± 0.0026	−204.9	135752
04A-7b	1945 ± 30	41 (p)	s	31	−25	0.7852 ± 0.0027	−214.8	135737
04A-7c	1920 ± 30	41 (p)	s	31	−25	0.7873 ± 0.0027	−212.7	135738
04A-8a‖	1755 ± 40	41 (p)	s	31	−25	0.8035 ± 0.0037	−196.5	135739
04A-8b	2040 ± 25	41 (p)	s	31	−25	0.7758 ± 0.0023	−224.2	135997
04A-11a	1865 ± 30	41 (p)	s	30	−27.9	0.7928 ± 0.0026	−207.2	135740
04A-11a rep	1920 ± 30	41 (p)	s	30	−27.9	0.7872 ± 0.0026	−212.8	135753
04A-11b	1840 ± 30	41 (p)	s	30	−28	0.7954 ± 0.0027	−204.6	135741
04A-11c	1895 ± 30	41 (p)	s	30	−28	0.7899 ± 0.0029	−210.1	135742
04A-21‖	1345 ± 35	45 (l)	s	24	−25	0.8459 ± 0.0033	−154.1	135743
04A-47	2370 ± 35	45 (l)	s	16	−25	0.7446 ± 0.0029	−255.4	135744
04A-56a‖	1435 ± 30	45 (m)	s	109	−26.9	0.8362 ± 0.0027	−163.8	135745
04A-56b‖	1415 ± 25	45 (m)	s	109	−27	0.8386 ± 0.0023	−161.4	135746
04A-57a‖	1565 ± 25	45 (m)	s	110	−26	0.8230 ± 0.0025	−177.0	135747
04A-57b‖	1450 ± 30	45 (m)	s	110	−26.1	0.8347 ± 0.0030	−165.3	135748
04A-74b	2175 ± 25	41 (p)	s	108	−27	0.7630 ± 0.0020	−237.0	135749
04A-76a‖	1700 ± 35	45 (o)	s	112	−25	0.8095 ± 0.0031	−190.5	135750
04A-76b‖	1660 ± 30	45 (o)	s	112	−26.8	0.8133 ± 0.0026	−186.7	135751

*a,b,c indicate split of a sample; rep indicates an additional run of a sample.

[†]±1σ-age in radiocarbon years using the Libby half-life of 5568 yr and following the conventions of Stuiver and Polach (1977).

[‡] δ13C values are the assumed values according to Stuiver and Polach (1977, p. 355) when given without decimal places. Values measured for the material itself are given with a single decimal place. Samples from the same horizon that did not have a sample specific δ13C analysis (e.g., 04A 7b, 04A 7c vs. 04A 7a were given the same δ13C value with an uncertainty of ±1%).

[§]All ages obtained by AMS analysis at the Center for Accelerator Mass Spectrometry (CAMS), Lawrence Livermore National Laboratory, Livermore, California.

‖Included in the final Oxcal model (Fig. 4).

Table 2
Ages of Earthquakes along the Southern Hayward Fault at Tyson's Lagoon

Event	Age Ranges (yr, A.D.) 68 Percentile		Age Ranges (yr, A.D.) 95 Percentile		Mean Age * (yr A.D.)	Mean Interval * (yr)	Interval Range, 95 Percentile (yr)
E1	1868	1868	1868	1868	1868		
						142 ± 38	82–212
E2	1695	1777	1657	1785	1725 ± 38		
						97 ± 49	8–191
E3	1587	1667	1536	1737	1629 ± 46		
						153 ± 59	37–274
E4	1425	1515	1385	1585	1475 ± 47		
						158 ± 62	36–280
E5	1265	1356	1238	1408	1317 ± 44		
						183 ± 85	25–337
E6	1032	1206	1005	1269	1134 ± 77		
						177 ± 79	36–318
E7	940	983	913	997	957 ± 21		
						135 ± 42	53–213
E8	769	852	757	899	822 ± 40		
						162 ± 41	93–241
E9	651	671	639	682	660 ± 10		
						216 ± 44	126–298
E9.5	397	485	366	532	444 ± 42		
						197 ± 57	85–311
E10	206	286	169	330	247 ± 40		
						156 ± 54	53–264
E11	54	134	11	172	91 ± 40		

*Single standard deviation (i.e., ±1 σ) derived from the probability density function output from Oxcal for each event. Calibration curve used: IntCal04, Northern Hemisphere (Reimer, *et al.*, 2004).
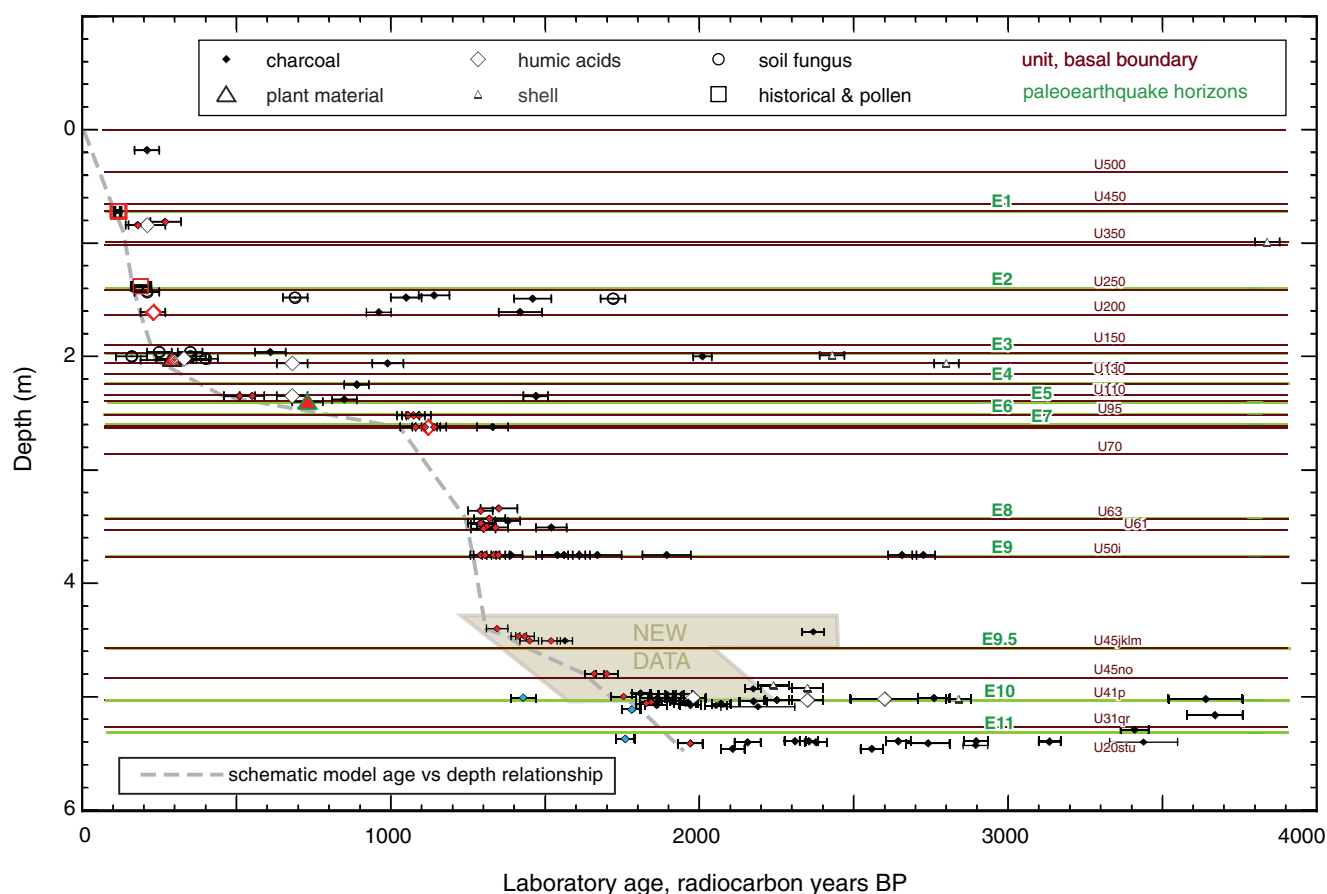
Figure 3. Scatter plot of uncalibrated radiocarbon ages ($\pm 1\sigma$) in stratigraphic sequence by depth below the ground surface. Positions of event horizons relative to the stratigraphic levels are shown as green lines labeled E1 through E11. Depths of samples plotted normalized to a standard section. Symbols in red indicate samples used in the chronological model shown in Figure 4. Blue samples are excluded, as discussed in the text.

offset. (3) In trench 01A (south wall, m9), a pronounced (0.12 m) offset of the base of u45 does not extend to the higher contacts within unit u45. (4) In trench W2 (south wall, m4; Lienkaemper *et al.*, 2003, sheet 8), a fault trace with little (<0.02 m) or no apparent vertical offset extends upward to u45 (subunit O). This last location may be evidence for ground shaking rather than fault rupture, but may nonetheless be relevant to the approximate timing of the earthquake. We regard these five upward terminations as additional supportive evidence for E9.5, realizing that one should be cautious about relying only upon the upward die out of ruptures (Bonilla and Lienkaemper, 1990; Scharer *et al.*, 2007).

Finally, there is clear evidence of an erosional unconformity at the E9.5 horizon, not only at the main fault trace as described previously, but also within the pond as described in the next section. This suggests that an abrupt general relative uplift adjacent to the pond at the time of E9.5 drove this erosion, which is not consistent with the slower process of creep.

In summary, our evidence for an earthquake E9.5 located within unit u45 includes two scarp colluviums that over-

lie the traces of the main fault zone, which are part of a general erosional unconformity. Additionally supporting E9.5 are five fault strands that die upward within u45 (one of which terminates directly beneath a blocky scarp colluvium), and the older u45 in trench 02A is tilted and overlain by subhorizontal younger u45. In clear contrast, earthquake E9 occurred after the deposition of all of unit u45. This is most clearly shown by a fault flower structure at the top of unit u45 illustrated in Figure 2d (from LW07, fig. 5), so it is reasonable to conclude that E9.5 is a different rupture. Additionally, trench 02A (Fig. 2b) shows twice as much vertical separation on the E9.5 colluvium (0.26 m) compared with that on the E8 horizon (0.13 m, on u61), thus suggesting substantial slip occurring in E9. Unfortunately, at the main fault trace, much of the evidence for E9 has been eroded away, so no blocky colluvium was preserved in any of our exposures. This is the main reason that event E9.5 was not originally recognized as a separate event. Additionally, although the scarp colluvium in trench 02A was logged fully in the field, final drafting (LW07) omitted this level of detail, causing us to overlook this critical evidence of E9.5 at that time.
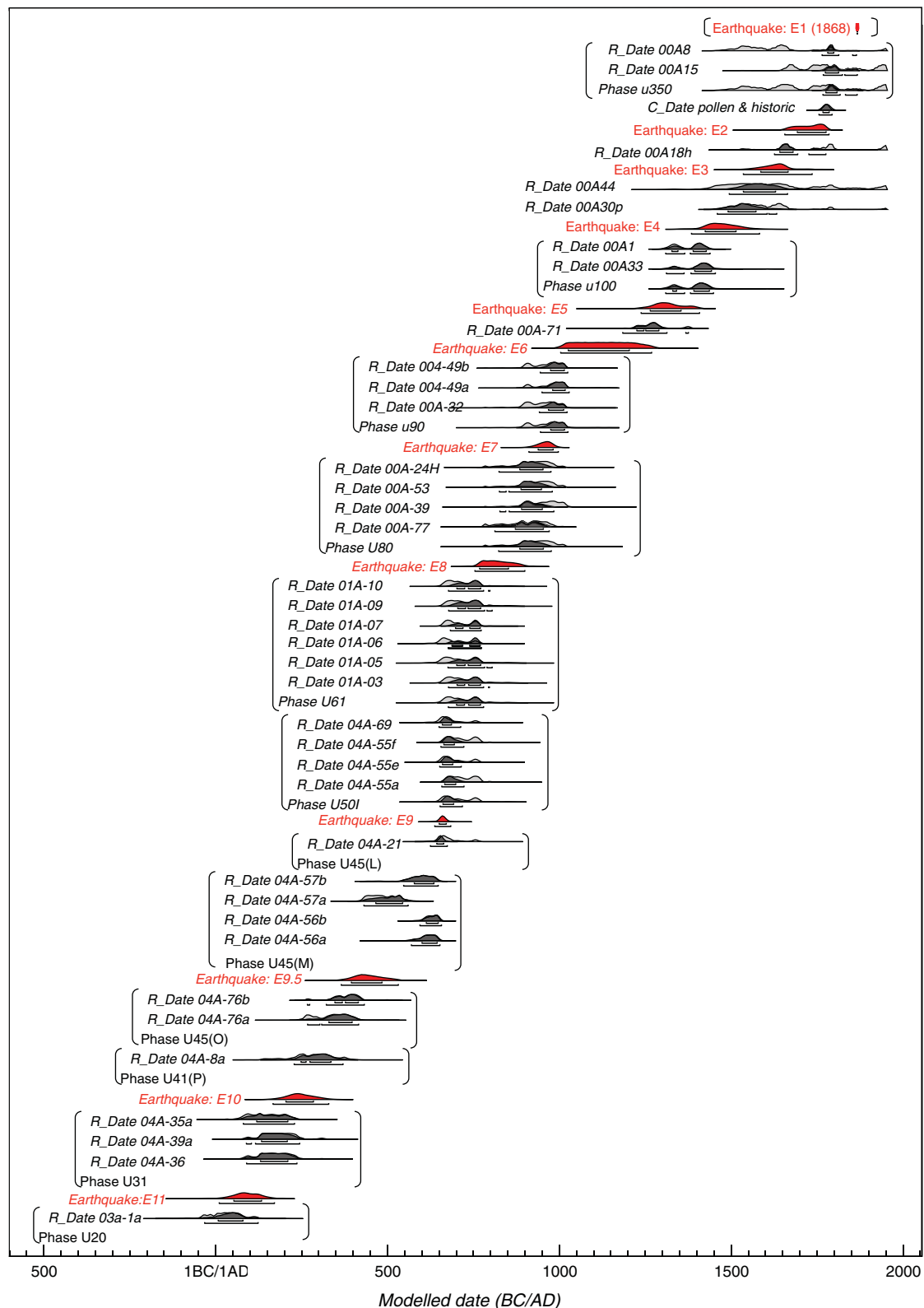
Figure 4. Calibrated age distributions of radiocarbon samples and paleoearthquakes using samples marked in red in Figure 3 calculated using OxCal, v. 4.0 (Bronk Ramsey, 1995, 2001, 2007). Outlined light gray areas show prior probability distribution functions of calibrated radiocarbon ages of samples; dark gray areas show posterior distributions. Red areas represent the probability distributions calculated for the paleoearthquakes. Lines below each distribution show limits of the 95.4- and 68.2-percentile confidence ranges for these distributions. Sample material is detrital charcoal except where noted. Earthquake ages were calculated using Oxcal's Date function.
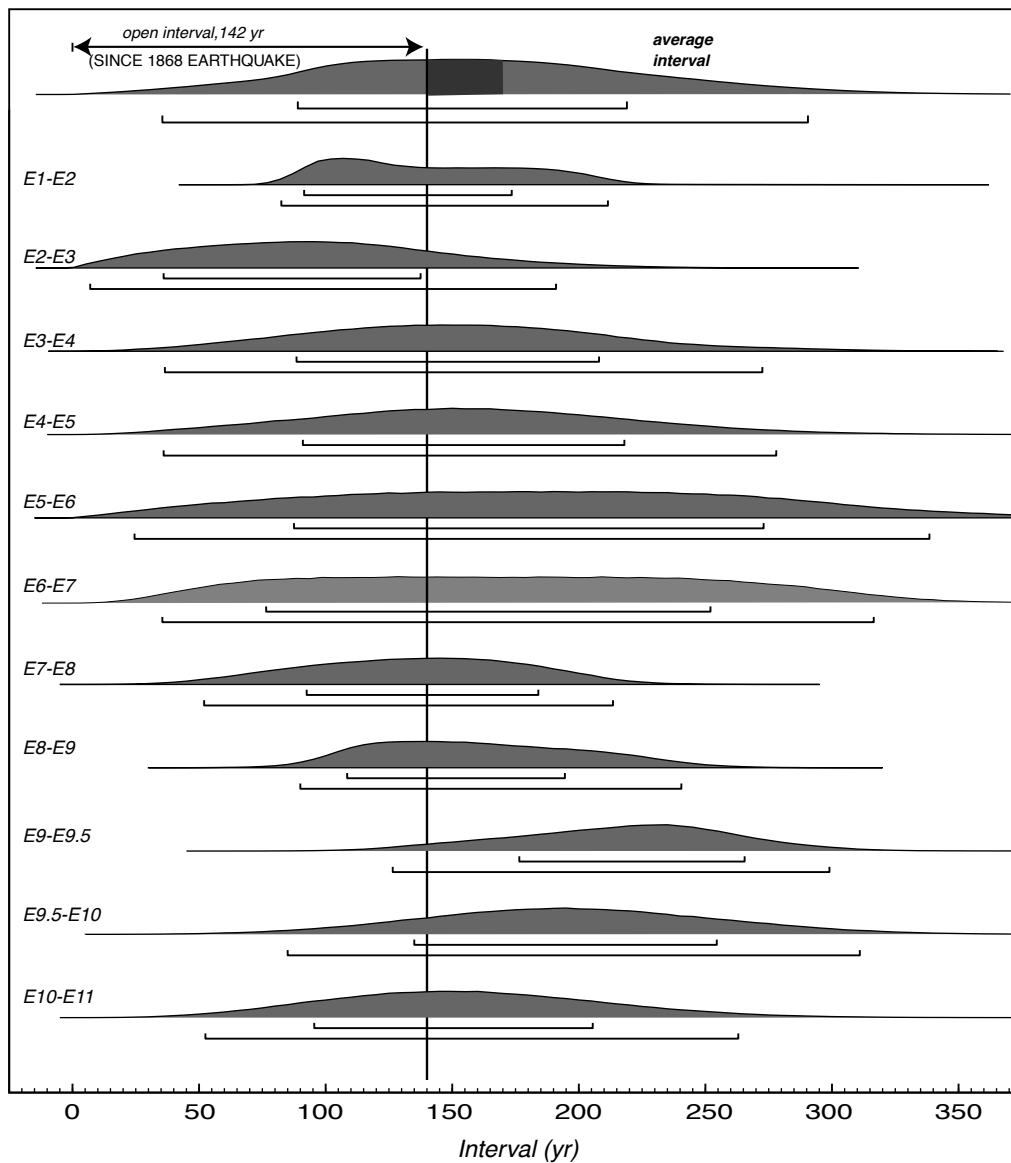
Figure 5. Probability density functions (PDFs) of 11 individual intervals and average interval between the earthquakes, resulting from Monte Carlo selection of intervals from the Oxcal-generated age PDFs. The upper bar under each PDF indicates the 68-percentile confidence range and the lower bar indicates the 95-percentile confidence range. Plot of the average interval illustrates calculation of the 30-yr conditional probability: Dark gray area highlights area of PDF over the next 30 yr, which divided by all areas to the right of the open interval yields a probability of 29%.

Stratigraphic Control on E9.5

In Figure 2d a fault flower structure indicating a surface rupture horizon at the unit u45–u50 contact shows that event E9 is distinctly younger than all subunits of unit u45. In contrast, the presence of scarp colluvium entirely within the lower part of u45 clearly indicates that a different event horizon, E9.5, lies well below the top of the unit (Fig. 2a,b) on an erosional unconformity that we show as younger u45 overlying older u45. We have much more detailed information about the history of deposition and subsequent erosion within unit u45 on the east side of the pond. Figure 2c illustrates the erosional unconformity in the lower part of u45 to

clarify details of stratigraphy and age control (see Fig. 1 for location). The older u45 (subunits O, N) and much of u41 were eroded away within the pond, and younger u45 (subunits M, L, K, J) were deposited directly on u41 across the entire pond. The timing of this erosional unconformity is also consistent with uplift in E9.5. Trench 04A (Lienkaemper et al., 2005) shows that unit M thins near the east edge of the pond, appears only sporadically in lenses, until disappearing by midway across the pond. Sandy silt units L and J are separated by a dark clayey silt K, which thins and pinches out near the west side of the pond. Thus, at the main 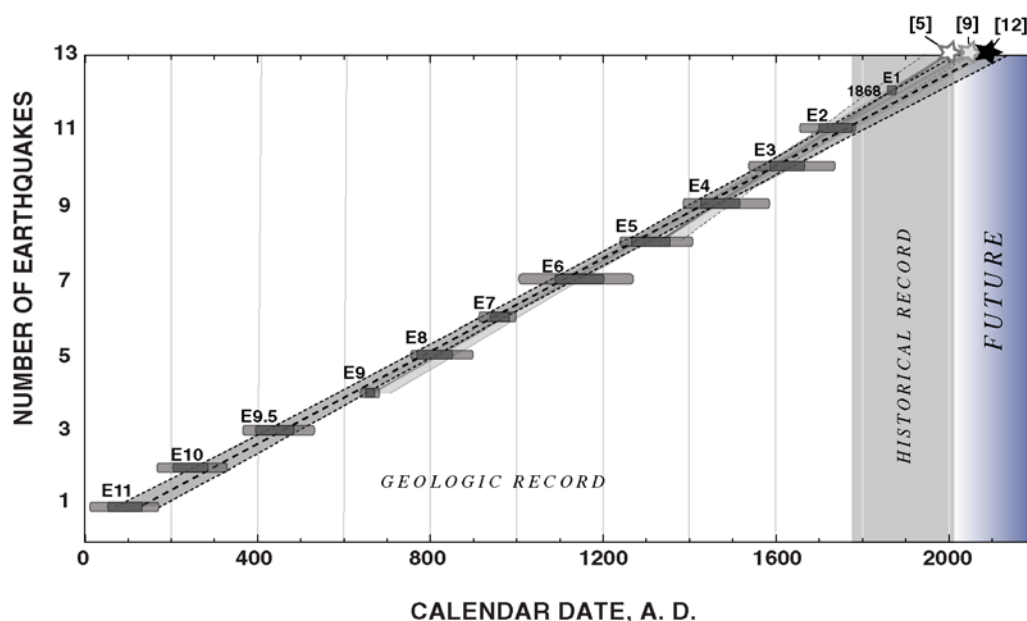trace the younger u45 is represented by undifferentiated subunits L and J. We reason that the older u45 at the main trace

Figure 6. Summary of age ranges for all 12 earthquakes. Confidence ranges are shown by darker bars for the 68.2 percentile and by the lighter bars for the 95.4 percentile. Stars indicate the expected dates of the next earthquakes using projections of linear regressions of earthquake ages in our model for the 5 most recent events (white star, 2008), the 9 most recent events (2056), or all 12 events (solid black star, 2096).

also is probably composed of the two subunits (O, N) shown to be present within the pond at the time of the major erosional event shown in Figure 2c. For age control of the earthquake sequence, it is important to be aware that while the younger u45 is physically composed of u45 (L, J), the age of the erosional unconformity, and thus the E9.5 event horizon, lies between u45 subunits M and N.

Revised Earthquake Chronology

The Oxcal model (Table 2, Fig. 4), revised from LW07, reflects the addition of the new radiocarbon data from units u41 and u45 (Table 1, Fig. 3) and inclusion of event E9.5 between younger u45 subunits (J, K, L, M) and older subunits (N, O). Figure 3 shows the laboratory dates of all radiocarbon samples; those used in the final Oxcal model (Fig. 4; Ⓔ model available in the electronic edition of BSSA) are colored in red. In our earlier papers (L02, LW07), we chose to group some samples using the SUM function in Oxcal, mainly because most of these represented charcoal from burn layers that had highly clustered laboratory ages. Hence, these radiocarbon dates were treated as if they were multiple estimates from the same sample. Current practice generally recommends grouping of all samples from the same stratigraphic horizon using the Phase function (Lienkaemper and Bronk Ramsey, 2009). This choice has had no significant impacts on the model in this particular case. We changed the model above E9 so that Phase is now used exclusively instead of Sum, but this caused no changes in the event ages in excess of 5 yr. For earthquake age determination, L02 used the Oxcal function Event, but this function was superseded

by the Date function in LW07 (because more recent versions of Oxcal do not include the Event function) and also in the model presented here. The two functions, Event and Date, do not produce any significant differences (< 10 yr) for the earliest events compared with L02; however, the lower age limit of E4 changed because of various other changes introduced in the lower part of the model.

Because detrital charcoal is often much older than the time of its deposition within the layer, we ran Oxcal to calibrate all of the laboratory radiocarbon dates and made use of Oxcal's statistical criterion for rejecting samples that are stratigraphically inconsistent with the chronologic model as a whole (e.g., agreement index A should usually exceed 60%; samples with lower agreement have little impact).

The initial runs of the Oxcal model with the new data (Table 1) indicated that three young samples below u45 now had unusually poor agreement indexes (A) (i.e., poor is defined in Oxcal as $A < 60\%$; rejected samples had A values of: W2–34, 0.7%; W2–29, 49%; W1–83, 10%; samples are colored blue in Fig. 3). Generally, the youngest radiocarbon dates are considered more reliable when sampling and dating are done correctly. However, we now have several consistent dates from burn layers within unit u45, which clearly indicate that u45 is actually older than a single previously dated sample (W2–34) collected from underlying unit u41. These new samples from u45 and u41 were selected under microscope at 36X and 72X magnification for the youngest appearing fraction of plant structure, selecting twigs, small fibrous plant material (i.e., not woody), or outermost growth rings. Also inspection at high magnification (> 50X) allowed exclusion of a form of black soil fungus, fairly common at the site,

which closely resembles charcoal at lower magnification. We had previously dated such fungus, showing that it can yield ages considerably younger than the time of deposition (L02). Consequently, in the current model, the three charcoal samples from three underlying units (u41, u31, and u20) were judged excessively young. Possible reasons include +errors in field sampling (such as sampling from a burrow, lab error, or as we think most likely the inadvertent sampling of black soil fungus). All three rejected samples were collected and run during the earlier period of investigation before all specimens were routinely checked at high magnification. In the following paragraph, we comment on the impact of these excluded samples on the critical result, the mean recurrence interval.

Because the new Oxcal model (Fig. 4) is unchanged above event E9, the age estimates for all younger events are essentially unchanged. The inclusion of new data has dramatically improved the constraint on E10. Intervals between individual events, however, remain poorly constrained (Table 2, Fig. 5), with the average of all 12 intervals ranging from 35 to 291 yr (95-percentile confidence).

For clarity in the following discussion, we use the term 1σ to mean the standard deviation of the average interval as determined by our Oxcal model with its distribution shown in Figure 5. We use the abbreviation SEM to distinguish the standard error of the mean recurrence interval (RI). We approximate SEM using the mean intervals in Table 2. The mean RI for the new 12-event model is 161 ± 10 yr (SEM; $1\sigma = 65$ yr; median, 158 yr); for the nine most recent events, 151 ± 10 yr (SEM); and for the five most recent, 138 ± 14 yr (SEM). If the three excluded young samples are put back into the model (despite poor agreement indices), then the mean 12-event RI becomes 155 ± 10 yr (SEM, $1\sigma = 64$ yr, median 148 yr). The new 161-yr mean RI is only slightly lower (by 9 yr) than the previous 11-event model (LW07). However, more significantly, the coefficient of variation (COV, the ratio of the mean RI to its standard deviation), has decreased from 0.48 to 0.40.

Discussion

Clearly it is important to the understanding of the Hayward fault that our earthquake chronology be as complete as possible; however, when compared with our prior results, we cannot claim the new chronology makes substantial impact on evaluations of seismic hazard. Our previous mean RI, based on an 11-event model, was 170 ± 14 yr (SEM) compared with 161 ± 10 yr in our revised model based on 12 events, and thus is indistinguishable within the errors. However, we suggest that the reduction in the COV from 0.48 to 0.40 may be of more general importance to the understanding of earthquake process, at least for relatively weak faults that have a major aseismic component of strain release. In the following paragraphs we revisit the subject of possible changes in the Hayward fault recurrence rate

over time and also how the new model changes estimates of the probability of future earthquakes.

Also similar to our previous report, the mean RI of 161 ± 65 yr (1σ), based on a 12-earthquake chronology, is essentially identical to the WG03 calculated mean RI of 161 yr (99–283 yr, 95 percentile) for the southern Hayward fault, which they derived from a complex geophysical model. WG08 used a similar value, a mean RI of 158 yr (112–219 yr, 95 percentile). This value was obtained directly from geologic data, relying on a preliminary version of our paleoseismic chronology.

Because the mean RI for only the past five events (138 ± 59 yr) is similar to the modern quiescent period (i.e., 142-yr open interval since the 1868 rupture, Fig. 5), it has attracted considerable public attention. We note, however, that the 5-event and 12-event mean RI values are not distinguishable at the 95-percentile confidence level, and differences could be explained by natural variability. Interestingly, the rate of earthquakes may also be greater between E9 and E6, allowing that periods of higher earthquake frequency may characterize this fault. A look at Figure 6, which summarizes the 12-event earthquake sequence, helps us examine the physical implications of having a shorter mean RI, as is suggested for the five most recent earthquakes. One possible reason for a shorter interval might be that the earlier part of the record remains incomplete; for example, another event would further reduce the 1900-yr mean RI to 148 yr. Another possibility is that the RI for the five most recent events is truly lower than the average for the longer record, perhaps because the 1868 earthquake occurred early (i.e., earlier than expected by the regression), due to high regional stress in the decades preceding the great 1906 earthquake; now, in a plausible post-1906 stress shadow (Reasenberg et al., 2003), some relative delay may be expected in the next southern Hayward fault earthquake. Interestingly, by simple linear regression of the full 12-event data set, the expected time for the next earthquake is the year 2096, which is delayed nearly 70 yr as compared with simply adding the mean RI of 161 to 1868. In contrast, a regression of just the past five events gives an expected mean occurrence time for the next earthquake of 2008.

As was discussed in L02, given available information about the long-term rates of creep and geologic slip on the Hayward fault, it is difficult to reconcile earthquakes as large as the M 6.8 1868 earthquake (Bakun, 1999), occurring at such short recurrence intervals. Specifically, if the estimated 1868 average slip of 1.9 m (Yu and Segall, 1996) were a result of loading at the long-term geologic slip rate of 0.009 m/yr (Lienkaemper and Borchardt, 1996), then 211 yr of loading would be required. Consequently, to achieve any of the mean RI from our models of the past 1900 yr (ranging from 138 to 161 yr), there must either have been some earthquakes with significantly less slip than estimated for the 1868 earthquake, the 1868 slip was somewhat smaller, or the slip rate for the southern Hayward may vary at the

limit of the resolution of this study over a few centuries or millennia.

We estimate the current 30-yr conditional probability for a surface-rupturing earthquake on the southern Hayward fault (HS) at 29% by applying the probability density function (PDF) for the average interval for 12 events from the Oxcal model (probability calculation described in Fig. 5 caption), which is thus a time-dependent probability. This differs little from the LW07 estimate of 26% based on 11 events. We estimate uncertainty in this probability (using $\pm 2 \times$ SEM of the RI) by comparison with the Gaussian or normal distribution, nearly identical (see Fig. 7) to the PDF of the average interval shown at the top of Figure 5, which gives $28 \pm 6\%$. In contrast, a time-independent Poisson estimate of 30-yr probability is only $17 \pm 2\%$. The Brownian passage time, or BPT model (Matthews *et al.*, 2002), is another method for estimating time-dependent probability of earthquakes with a functional form including a period of quiescence following the previous large earthquake, with increasing likelihood toward a mean, but it also requires that extremely long RI may occur. Parsons (2008) modeled the larger uncertainty ranges from our incomplete LW07 (11-event) chronology, estimating that a BPT function with a mean of 210 yr and COV of 0.6 could plausibly fit such uncertain intervals. We emphasize that the LW07 model included much larger intervals and uncertainties for events E9–E11 and did not include event E9.5. We expect a rerun of the Parsons (2008) method with our complete 12-event model would yield somewhat lower values for both COV and mean RI. For comparison, in Figure 7 we show a range of BPT distributions plotted together with the average interval from our 12-event

Oxcal model. The BPT with a mean of 180 yr (COV 0.4) agrees best with the central part of the average interval PDF, whereas a 210-yr mean (COV 0.6) for BPT fits the entire PDF quite poorly. We suggest that the BPT model may fit the Hayward fault chronology more poorly than a simple Gaussian distribution, because the fault is smoother than most faults (its largest bend is 0.7 km in a fault length of > 80 km), and it is so greatly weakened by creep release ($\sim 40\%$ aseismic, WG03) that it seems physically unlikely for it to go many centuries without failure in a large earthquake. Finally, we note that the COV of the southern Hayward fault appears to be fairly regular at 0.40 and relatively stable over time (0.42 or 0.43 for the most recent nine events and five events, respectively), and compared with other faults has a moderate COV similar to the average of 0.44 ± 0.22 (68%-confidence interval) obtained by Ellsworth *et al.* (1999) for several historical and paleoearthquake sequences.

Another question relative to the use of BPT arises with short intervals (< 50 yr), which the Oxcal model allows. Given the irregular character of pond deposition (i.e., generally no annual layers), a few decades may typically pass between depositional events that are distinguishable as units. Thus, any evidence for two large earthquakes occurring within a few decades would usually be hard to distinguish. Given the large uncertainties in age calibration in the Oxcal model one cannot strictly eliminate the possibility of extremely short intervals. So in this respect the BPT models may be reasonably consistent with our Oxcal model, but no more so than a Gaussian distribution that is truncated at zero.

Conclusions

Adding a twelfth earthquake (E9.5) to the southern Hayward fault chronology only marginally increases its 30 yr conditional probability of future large earthquakes, from 26% to 29%, compared with the earlier chronology (LW07). However, because we believe this sequence to be complete for about two millennia, it now offers considerably more insight into the natural variation in earthquake recurrence intervals. Taken together, the addition of event E9.5 and the much-improved age control for the earliest earthquakes suggests considerable regularity for large southern Hayward fault earthquakes, thus strengthening the empirical basis for the use of time-dependent probability models for estimating seismic hazard at least for some faults.

Data and Resources

All data used in this paper came from published sources listed in the references.
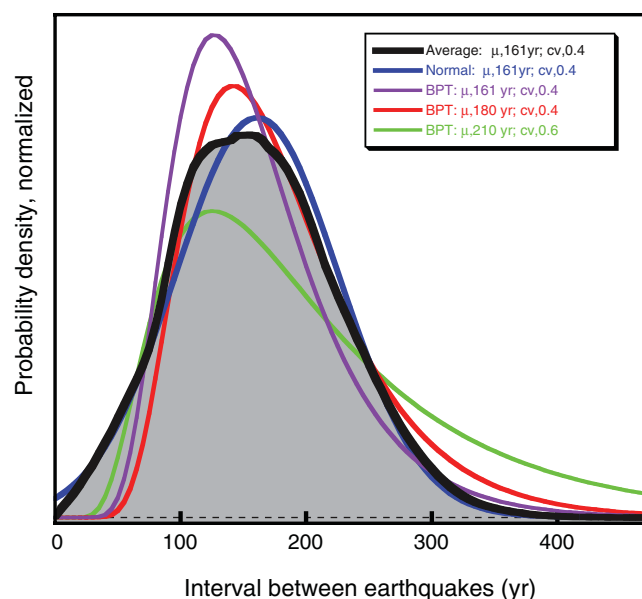

Figure 7. Comparison of probability density function (PDF) of the average earthquake recurrence interval for the southern Hayward chronology derived from the 12-event Oxcal model (gray area) to other distributions as discussed in the text.

Acknowledgments

References

Bakun, W. H. (1999). Seismic activity of the San Francisco Bay region, *Bull. Seismol. Soc. Am.* **89,** 764–784.

Bonilla, M. G., and J. J. Lienkaemper (1990). Visibility of fault strands in exploratory trenches and timing of rupture events, *Geology* **18,** 153–156.

Bronk Ramsey, C. (1995). Radiocarbon calibration and analysis of stratigraphy: The OxCal program, *Radiocarb.* **37,** no. 2a, 425–430.

Bronk Ramsey, C. (2001). Development of the radiocarbon calibration program OxCal, *Radiocarb.* **43,** no. 2a, 355–363.

Bronk Ramsey, C. (2007). *OxCal Program*, v. **4.0,** Radiocarbon Accelerator Unit, University of Oxford, U.K.

Ellsworth, W. L., M. V. Matthews, R. M. Nadeau, S. P. Nishenko, P. A. Reasenberg, and R. W. Simpson (1999). A physically-based earthquake recurrence model for estimation of long-term earthquake probabilities, *U.S. Geol. Surv. Open-File Rept. 99-522*, 23 pp. (http://geopubs.wr.usgs.gov/open-file/of99-522/).

Lienkaemper, J. J., and G. Borchardt (1996). Holocene slip rate of the Hayward fault at Union City, California, *J. Geophys. Res.* **101,** 6099–6108.

Lienkaemper, J. J., and C. Bronk Ramsey (2009). Oxcal: Versatile tool for developing paleoearthquake chronologies—A primer, *Seism. Res. Letts.* **80,** 431–434.

Lienkaemper, J. J., and J. S. Galehouse (1998). New evidence doubles the seismic potential of the Hayward fault, *Seism. Res. Letts.* **69,** 519–523.

Lienkaemper, J. J., and P. L. Williams (2007). A record of large earthquakes on the southern Hayward fault for the past 1800 years, *Bull. Seismol. Soc. Am.* **97,** 1803–1819.

Lienkaemper, J. J., T. E. Dawson, S. F. Personius, G. G. Seitz, L. M. Reidy, and D. P. Schwartz (2002a). A record of large earthquakes on the southern Hayward fault for the past 500 years, *Bull. Seismol. Soc. Am.* **92,** 2637–2658.

Lienkaemper, J. J., T. E. Dawson, S. F. Personius, G. G. Seitz, L. M. Reidy, and D. P. Schwartz (2002b). Logs and data from trenches across the Hayward fault at Tyson's Lagoon (Tule Pond), Fremont, Alameda County, California, *U.S. Geol. Surv. Miscellaneous Field Studies Map MF-2386*, 3 sheets, pamphlet 10 pp. (http://pubs.usgs.gov/mf/2002/2386/).

Lienkaemper, J., P. Williams, T. Dawson, S. Personius, G. Seitz, S. Heller, and D. Schwartz (2003). Logs and data from trenches across the Hayward Fault at Tyson's Lagoon (Tule Pond), Fremont, Alameda County, California, *U.S. Geol. Surv. Open-File Rept. 03-488*, 6 pp., 8 plates. (http://pubs.usgs.gov/of/2003/of03-488/).

Lienkaemper, J. J., P. L. Williams, R. R. Sickler, and T. E. Fumal (2005). Log of Trench 04A across the Hayward Fault at Tyson's Lagoon (Tule Pond), Fremont, Alameda County, California, *U.S. Geol. Surv. Open-File Rep. 2005-1350*, 2 plates. (http://pubs.usgs.gov/of/2005/1350/).

Matthews, M. V., W. L. Ellsworth, and P. A. Reasenberg (2002). A Brownian model for recurrent earthquakes, *Bull. Seismol. Soc. Am.* **92,** 2233–2250.

Parsons, T. (2008). Earthquake recurrence on the south Hayward fault is most consistent with a time dependent, renewal process, *Geophys. Res. Lett.* **35,** Citation L21301; doi 10.1029/2008GL035887, 5 pp.

Reasenberg, P. A., Th. C. Hanks, and W. H. Bakun (2003). An empirical model for earthquake probabilities in the San Francisco Bay region, California, 2002–2031, *Bull. Seismol. Soc. Am.* **93,** 1–13.

Reimer, P. J., T. A. Brown, and R. W. Reimer (2004). Discussion: Reporting and calibration of post-bomb C-14 data, *Radiocarb.* **46,** no. 3, 1299–1304.

Scharer, K. M., R. J. Weldon, T. E. Fumal, and G. P. Biasi (2007). Paleoearthquakes on the southern San Andreas fault, Wrightwood, California, 3000–1500 B.C.: A new method for evaluating paleoseismic evidence and earthquake horizons, *Bull. Seismol. Soc. Am.* **97,** 1054–1093.

Stuiver, M., and H. A. Polach (1977). Discussion; reporting of C-14 data, *Radiocarb.* **19,** 355–363.

Working Group on California Earthquake Probabilities (2003). Earthquake probabilities in the San Francisco Bay Region: 2002–2031, *U.S. Geol. Surv. Open-File Rept. 03-214*, 235 pp. (http://pubs.usgs.gov/of/2003/of03-214/)

Working Group on California Earthquake Probabilities, 2007 (2008). The Uniform California Earthquake Rupture Forecast, Version 2 (UCERF 2), *U.S. Geol. Surv. Open File Rept. 2007-1437*, Version 1.1. (http://pubs.usgs.gov/of/2007/1437/).

Yu, E., and P. Segall (1996). Slip in the 1868 Hayward earthquake from the analysis of historical triangulation data, *J. Geophys. Res.* **101,** 16,101–16,118.

U.S. Geological Survey 977
345 Middlefield Road
Menlo Park, California 94025
jlienk@usgs.gov
    (J.J.L.)

Department of Geological Sciences
San Diego State University
San Diego, California 92182
    (P.L.W.)

Center for Accelerator Mass Spectrometry
Lawrence Livermore National Laboratory
L-397 Livermore, California 94551
    (T.P.G.)